Active Polyhedron: Surface Evolution Theory Applied to Deformable Meshes

Greg Slabaugh, Gozde Unal
Intelligent Vision and Reasoning Department
Siemens Corporate Research
Princeton, NJ 08540

Abstract

This paper presents a novel 3D deformable surface that we call an active polyhedron. *Rooted in surface evolution theory, an active polyhedron is a polyhedral surface whose vertices deform to minimize a regional and/or boundary-based energy functional. Unlike continuous active surface models, the vertex motion of an active polyhedron is computed by integrating speed terms over polygonal faces of the surface. The resulting ordinary differential equations (ODEs) provide improved robustness to noise and allow for larger time steps compared to continuous active surfaces implemented with level set methods. We describe an electrostatic regularization technique that achieves global regularization while better preserving sharper local features. Experimental results demonstrate the effectiveness of an active polyhedron in solving segmentation problems as well as surface reconstruction from unorganized points.*

1 Introduction

Active surfaces, the 3D version of 2D active contours, are an essential component of many computer vision and image processing techniques. After a surface is initialized in 3D space, it is subjected to various forces to evolve (or deform) it to solve a variety of problems, such as segmentation, shape modeling, multi-view 3D reconstruction, and more.

1.1 Related work

In general, two representations of an active surface are commonly used: explicit and implicit. Explicit representations [4, 6, 10, 11, 14] have been used in numerous medical imaging problems, including the segmentation of anatomical structures from 3D ultrasound, which is our primary application. An important explicit representation is a mesh composed of triangles in 3D space, precisely the surface representation we employ in this paper.

While it is possible to model topological changes using an explicit surface representation, an advantage of the second major category of segmentation approaches, those based on implicit representations [1, 3, 9, 15], is that they can automatically change topology when necessary. In particular, the method presented in [1] uses statistical modeling of data inside and outside a contour to achieve ultrasound segmentation; however the amount of noise in the examples we segment is typically much larger.

Several other techniques for ultrasound segmentation that do not use deformable models also exist. For example, Boukerroui et al. [2] present a multi-resolution framework with estimation of local textural and acoustic features of the ultrasound data to increase robustness against speckle noise.

1.2 Our contribution

Although the function that controls the speed of each vertex in either the explicit or implicit schemes may depend on a local, regional, or global statistic or descriptor, the motion of each vertex is not coupled to its neighbor vertices or adjacent faces. In this paper, we present a polyhedral surface that we call an *active polyhedron*, which integrates these forces once more over the polyhedral faces, effectively providing a lowpass filtering effect on the data measurements. Consequently, the active polyhedron approach differs significantly from previous 3D active surfaces and offers increased robustness to noise, including speckle noise that is observed in ultrasound data. This type of noise is spatially correlated and contaminates pointwise image measurements. As a result, an active polyhedron is much less prone to segmentation errors resulting from local variations in the speed function, and in such cases, will be more effective at aligning its faces with the target structure. Compared with previous methods, our active polyhedron model prefers well-separated vertices since the information is being accumulated over adjacent faces of a vertex to determine its motion. This idea builds upon Unal et al.'s active polygon framework [12, 13], which accumulates 2D image information over adjacent edges of a 2D polygon's vertex.

In addition to contributing this active polyhedron model, we present the general theory describing its evolution by deriving the vertex motion using surface evolution theory. We also formulate the extension of 2D electrostatic regularization into 3D, which requires special attention to achieve the desired regularization.

The rest of this paper is organized as follows. In Section 2, we derive the vertex motion of an active polyhedron and discuss our 3D electrostatic regularizer. Next, in Section 3 we describe implementation details. Then, in Section 4 we present some experimental results that demonstrate the usefulness of the proposed method in solving segmentation problems as well as reconstruction from unorganized points.

2 Active Polyhedron

In this section we derive, for the first time, the equation of motion for an active polyhedron by minimizing an energy functional using gradient descent. This derivation is based on that of the 2D active polygon [13], however, is quite different due to the 3D surface we use and its parametrization.

We begin with a surface $\mathbf{S} : \mathbb{R}^2 \rightarrow \mathbb{R}^3$ around a region $R \subset \mathbb{R}^3$, as well as a function $f : \mathbb{R}^3 \rightarrow \mathbb{R}$, and use the divergence theorem to express the energy of the surface computed over R as a surface integral over ∂R,

$$E(\mathbf{S}) = \iiint_R f(x,y,z)dxdydz = \iint_{\mathbf{S}=\partial R} \langle \mathbf{F}, \mathbf{N} \rangle dS, \tag{1}$$

where $\mathbf{N}$ denotes the outward unit normal to $\mathbf{S}$, and $\mathbf{F}$ is chosen so that $\nabla \cdot \mathbf{F} = f$, dS is the differential area on the surface, the surface is parameterized by $\mathbf{S}(u,v) = (x(u,v), y(u,v), z(u,v))$, and $\langle \cdot \rangle$ is the inner product operator.

Next, we take the derivative of $E(\mathbf{S})$ with respect to a variable p whose variation affects the geometry of the surface, but is independent of the parametrization variables (u,v). This derivative can be shown [16] to have the form

$$E_p(\mathbf{S}) = \iint_{\mathbf{S}} f\langle \mathbf{S}_p, \mathbf{N} \rangle dS. \tag{2}$$

Equation 2 applies both to a continuous active surface as well as a surface discretely sampled using a polygonal mesh.

Let us now add the constraint that $\mathbf{S}$ be a mesh of N triangles. $\mathbf{S}_i$, the ith triangle of $\mathbf{S}$, can be parameterized as

$$\mathbf{S}_i(u,v) = \mathbf{v}_{1i} + u\mathbf{e}_{1i} + v\mathbf{e}_{2i}, \tag{3}$$

where points $\mathbf{v}_{1i}$, $\mathbf{v}_{2i}$, and $\mathbf{v}_{3i}$ are triangle vertices, triangle edge vectors $\mathbf{e}_{1i} = \mathbf{v}_{2i} - \mathbf{v}_{1i}$, $\mathbf{e}_{2i} = \mathbf{v}_{3i} - \mathbf{v}_{1i}$, and $u \in [0,1]$ and $v \in [0, 1-u]$ are the parametrization variables over

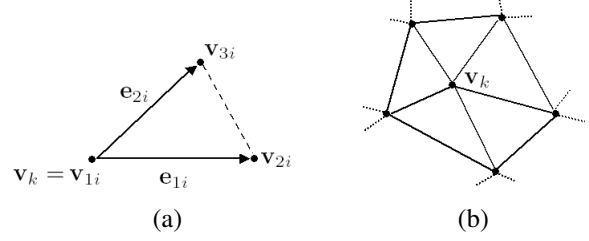(a)   (b)

Figure 1. The vertices and edges used in the parametrization of a triangle are shown in (a). Any point on the triangle can be expressed as $\mathbf{x}_i = (\mathbf{v}_{1i} + u\mathbf{e}_{1i} + v\mathbf{e}_{2i})$. In (b), $\mathbf{v}_k$'s neighbor triangles $\mathbf{D}_k$ are shown.

which the integrals in the equations below will be evaluated. A depiction appears in Figure 1(a).

With this parametrization, we can express Equation 2 as a sum of piecewise continuous integrals over the triangle faces,

$$E_p(\mathbf{S}) = \sum_{i=1}^{N} \iint_{\mathbf{S}_i} f(\mathbf{v}_{1i} + u\mathbf{e}_{1i} + v\mathbf{e}_{2i})\langle \mathbf{S}_{ip}, \mathbf{N}_i \rangle dS_i. \tag{4}$$

Next, we define $\mathbf{S}_{ip}$ for vertex $\mathbf{v}_k$ as

$$\mathbf{S}_{ip}(u,v,\mathbf{v}_k) = \begin{cases} (1-u-v)\mathbf{e}, & \mathbf{S}_i \in \mathbf{D}_k \\ 0, & \text{otherwise} \end{cases} \tag{5}$$

where $\mathbf{D}_k$ is the set of M surface triangles that neighbor vertex $\mathbf{v}_k$, as depicted in Figure 1(b), and $\mathbf{e}$ denotes one of the standard basis vectors for $\mathbb{R}^3$, (i.e., $[1,0,0]^T, [0,1,0]^T$, or $[0,0,1]^T$). We evaluate Equation 4 with p equal to one of coordinates of $\mathbf{v}_k$, yielding

$$\begin{aligned} E_p(\mathbf{S}) &= \sum_{\mathbf{S}_i \in \mathbf{D}_k} \iint_{\mathbf{S}_i} f(\mathbf{S}_i(u,v))\langle(1-u-v)\mathbf{e}, \mathbf{N}_i\rangle dS_i \\ &= \sum_{\mathbf{S}_i \in \mathbf{D}_k} \langle \mathbf{e}, \mathbf{N}_i \rangle \iint_{\mathbf{S}_i} (1-u-v)f(\mathbf{S}_i(u,v))dS_i. \end{aligned}$$

If we introduce a time variable t and evolve coordinates (x_i, y_i, z_i) in the gradient directions given above, we obtain the following gradient flow for the vertex $\mathbf{v}_k$,

$$\begin{aligned} \frac{d\mathbf{v}_k}{dt} &= \sum_{\mathbf{S}_i \in \mathbf{D}_k} \iint_{\mathbf{S}_i} (1-u-v)f(\mathbf{S}_i(u,v))dS_i \mathbf{N}_i \\ &= \mathbf{A}(\mathbf{v}_k) \end{aligned} \tag{6}$$

Equation 6 is an ordinary differential equation that describes the vertex motion of the active polyhedron. This equation can be computed using MK^2 operations, where K is the number of samples (in one dimension) on a triangle at

which the integration occurs. Note that Equation 6 is significantly different than previous models as the function f is integrated over triangular faces rather than applied pointwise. As we shall see, this integration of f provides added robustness to noise. Also note that the image-based data term f in Equation 6 is completely general, allowing one to design different flows for solving various problems.

2.1 Electrostatic Regularization

The flow of an active polyhedron may, under the sole influence of a data term, become irregular when a vertex becomes infinitesimally close to a non-neighbor face of the polyhedron. To address this issue, we incorporate a natural regularization term introduced in [13] that is based on electrostatic principles. However, the 3D version of this regularization requires special attention so that it achieves the desired effect.

The electrostatic regularization technique models a uniform charge density λ along each surface triangle. This charge density induces a global electric field $\mathbf{G} \in \mathbb{R}^3$ that applies a repulsive force at each vertex. To compute the electric field at a general point $\mathbf{p} \in \mathbb{R}^3$, we must consider the differential electric field $d\mathbf{G}(\mathbf{p})$ exerted by a charged particle at location $\mathbf{x}_i$ on triangle $\mathbf{S}_i$. As given by Coulomb's law [7], the electric force is inversely proportional to the square of the Euclidean distance $||\mathbf{p} - \mathbf{x}_i||^2$ between the charged particles, and directed along the vector $(\mathbf{p} - \mathbf{x}_i)/||\mathbf{p} - \mathbf{x}_i||$.

$$\mathbf{G}(\mathbf{p}) = \sum_{i=1}^{N} \iint_{\mathbf{S}_i} \lambda \frac{\mathbf{p} - \mathbf{x}_i}{||\mathbf{p} - \mathbf{x}_i||^n} dS_i, \tag{7}$$

where $\mathbf{x}_i = (\mathbf{v}_{1i} + u\mathbf{e}_{1i} + v\mathbf{e}_{2i})$ is a point on $\mathbf{S}_i$, and $n = 3$.

While using $n = 3$ in Equation 7 will impart a repulsive force to a surface vertex, it fails to become singular as the vertex approaches the surface. This can be easily demonstrated if one considers a vertex $\mathbf{p} = [0, 0, z]^T$ directly above a disk of uniform charge and radius r as depicted in Figure 2. In this case, basic electromagnetics tells us the electric field is

$$\mathbf{G}(\mathbf{p}) = 2\pi\lambda \left(1 - \frac{z}{\sqrt{z^2 + r^2}} \right) \hat{\mathbf{z}}, \tag{8}$$

and thus

$$\lim_{z \to 0} \mathbf{G}(\mathbf{p}) = 2\pi\lambda\hat{\mathbf{z}}. \tag{9}$$

Instead, we would prefer an electric field that goes to infinity in the limit as the vertex moves towards the charged surface in order to prevent the surface from self-intersecting. To accomplish this, we set $n = 4$ in Equation 7. It is simple to verify that using $n = 4$ satisfies this requirement.
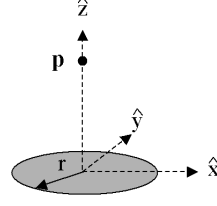

Figure 2. Electric field of a disk of charge.

There are several ways to make use of the electrostatic force to displace vertex $\mathbf{v}_k$ to regularize the surface. Perhaps the most thorough method would be to integrate the field $\mathbf{G}$ at each point $\mathbf{p} \in \mathbf{D}_k$, weighted by $(1 - u - v)$ so that points closer to $\mathbf{v}_k$ contribute more to the regularization, i.e.,

$$\frac{d\mathbf{v}_k}{dt} = \sum_{j=1, \mathbf{S}_j \in \mathbf{D}_k}^{M} \iint_{\mathbf{S}_j} (1 - u - v)\mathbf{G}(\mathbf{x}_j)dS_j, \tag{10}$$

where each $\mathbf{G}(\mathbf{x}_j)$ is computed over the L triangles $\mathbf{C}_k = \mathbf{S} \setminus \mathbf{D}_k$ (to avoid unwanted infinities). However, for each vertex, such an approach requires solving sums of quadruple integrals, which has computational complexity of LMK^4 operations.

To reduce the computational load, we instead choose to compute the vertex displacement as

$$\frac{d\mathbf{v}_k}{dt} = \mathbf{B}(\mathbf{v}_k) = \sum_{i=1, \mathbf{S}_i \in \mathbf{C}_k}^{L} \iint_{\mathbf{S}_i} \lambda \frac{\mathbf{p} - \mathbf{x}_i}{||\mathbf{p} - \mathbf{x}_i||^4} dS_i, \tag{11}$$

which, for each vertex, has computational complexity of LK^2 operations. We have found that in practice this simplified approach offers sufficient regularization and is reasonably fast. This electric force is designed to be insignificant when $\mathbf{v}_k$ is not very close to the surface triangles in $\mathbf{C}_k$, but becomes influential, even dominant, when the vertex gets very close to triangles in $\mathbf{C}_k$.

Note that this regularization approach differs significantly from standard methods such as Laplacian smoothing, which tend to shrink the surface and often produces overly smooth rounding at points of high curvature.

3 Implementation

3.1 Flow

We combine Equations 6 and 11 to yield the vertex flow

$$\frac{d\mathbf{v}_k}{dt} = \alpha\mathbf{A}(\mathbf{v}_k) + (1 - \alpha)\mathbf{B}(\mathbf{v}_k), \tag{12}$$

where α is a constant that weights the data term relative to the regularization term. In practice, we have found a value of $\alpha = 0.95$ to offer good performance. With this heavier weight on the data term, the regularization only contributes significantly to the flow when degeneracy occurs, allowing for the data term to govern the evolution during most of the evolution. Since updating a single vertex requires $(L + M)K^2 = NK^2$ operations, the computational complexity of our model is $N^2 K^2$ operations for each time step.

3.2 Mesh Operations

While the surface is deforming, it is necessary to perform some mesh operations to ensure that the mesh has a proper vertex distribution. Towards this goal we implement some standard mesh operations:

1. **Edge split.** This operation splits any edge whose length goes above a maximum length. A new vertex is placed at the center of the edge, and each triangle that included the edge is split into two, as shown in Figure 3.

2. **Edge collapse.** This operation collapses any edge whose length goes below a minimum length. The two vertices that comprise the edge are merged to one vertex, as shown in Figure 3.

3. **Face split.** During evolution, the magnitude of the image force applied to each face is computed. If face splitting is enabled, the triangle with the largest magnitude force is split into three triangles by placing a new vertex at the triangle center, as shown in Figure 3. The intuition here is that the edges with higher image speeds are close to image structures that may require finer details. Face splitting is enabled periodically during the surface flow.

These operations allow the surface to grow and to shrink; however, topological changes are not currently supported in our implementation. For many applications this is an advantage rather than a disadvantage. Techniques such as [5] require special algorithms to keep the topology of the level-set surface simple because it is very easy for implicit surfaces to break or leak to surrounding unrelated regions while propagating. This is not a problem for our model. On the other hand, topology adaptivity can be added to an active polyhedron as has been done in other mesh-based approaches such as [8, 11].

3.3 Speed term

3.3.1 Region-based functional for segmentation

As mentioned previously, the image-based speed term f described in Equation 6 has a general form that can be cus-
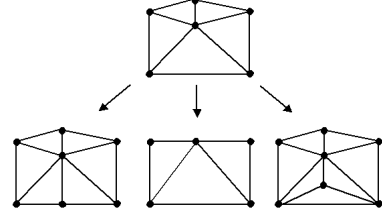

Figure 3. Mesh operations. The topmost mesh is refined using the edge split operator (lower left), edge collapse operator (lower center) and face split operator (lower right).

tomized for specific tasks. For image segmentation, we employ the piecewise constant region-based energy functional that uses mean statistics [3],

$$f(\mathbf{x}) = -(I(\mathbf{x}) - m_i)^2 + (I(\mathbf{x}) - m_o)^2, \quad (13)$$

where I is the 3D image, $\mathbf{x}$ is a point on the surface, m_i and m_o are the mean values of I inside and outside the polyhedron, respectively. This speed function is well suited to the segmentation of noisy images, as it does not rely on the image gradients. The voxels inside and outside the surface are found via scanline rasterization of the polyhedron.

3.3.2 Boundary-based functional for reconstruction from unorganized points

For reconstructing surfaces from unorganized points, we follow the example of [15] who implement a gradient flow on a distance volume to find the minimal distance surface. That is,

$$f(\mathbf{x}) = -\nabla D(\mathbf{x}) \cdot \mathbf{N}(\mathbf{x}), \quad (14)$$

where D is a distance volume formed by placing the unorganized points into a volumetric grid and computing the unsigned distance at each voxel to the closest unorganized point, and $\mathbf{N}$ is the surface normal.

4 Experimental Results

We now present experimental results showing an active polyhedron's ability to segment 3D image data and to reconstruct surfaces from unorganized points.

4.1 Validation

First, we validate the active polyhedron using ground truth data. For comparison, we also produce results using continuous active surfaces implemented with level set methods.

Our first example consists of a 128^3 volume of synthetic ultrasound data. The data suffers poor contrast and corruption by speckle noise, a common form of ultrasound noise resulting from coherent backscattering of echo signals. Inside the volume is a darker cylindrical structure of radius 10 units and height 64 units that simulates a blood vessel. We segment this data by placing a cube inside and at one end of the vessel, and evolve the active polyhedron using the speed term of Equation 13 and the electrostatic regularizer. Figure 5 shows the evolving active polyhedron for $t = 0, 10, 20, 30$, and 35 iterations, upon which the surface converged. On the right of Figure 5 we show the segmentation result achieved with the same data term and a curvature-based regularizer using a continuous active surface implemented with level set methods. Notice that result obtained with the active polyhedron is much smoother due to the integration of the data term along each triangle face, compared to the pointwise motion of the continuous active surface, which suffers multiple topology changes and leaking due to the speckle. Although it is possible to increase the regularization of the continuous active surface, doing so results in unsatisfactory results as the data term becomes ineffective in being attracted to target image features. The active polyhedron model produces better segmentation results, as is visually apparent in 2D slices of the volume, shown in Figure 4. Furthermore, in Table 1 we compute the surface area and volume of the segmentation results and compare them to the ground truth. The erratic shape of the continuous active surface results in over twice the actual surface area, while the active polyhedron more faithfully represents the shape.

In Figure 6 we reconstruct sphere from point cloud data. We generated a "clean" set of 625 points by sampling the equation of radius $= 15$ sphere to produce the point cloud on the top left of the figure, and in the bottom left of the figure we perturbed each point by adding zero-mean Gaussian distributed noise in the range $[-10, 10]$ to each coordinate of each vertex and adding 5% outliers uniformly distributed in the volume to produce a "noisy" point cloud. We embedded the point cloud in a 64^3 grid and formed an unsigned distance volume. The middle figures show the result of reconstructing a surface from the unorganized points using a level set implementation and Equation 14 with a curvature-based regularizer, while the right figures show the result of using the active polyhedron, Equation 14, and the electrostatic regularizer. As expected, the reconstruction of the clean data results in a polyhedral representation of a sphere. The reconstruction of the noisy data shows the susceptibility of the continuous active surface to local noise variations. However, the active polyhedron produces a smoother, more spherical surface due to its integration of the speed terms on the polygonal faces.
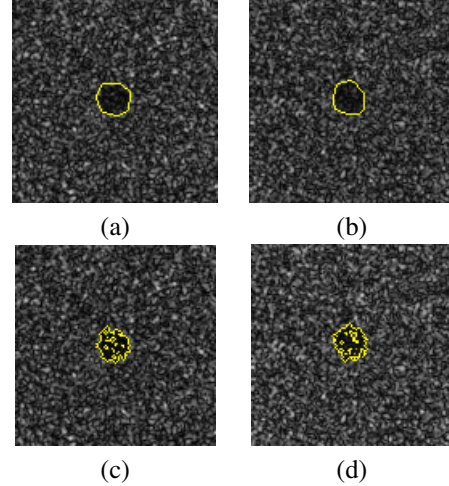

(a)　　　　　(b)

(c)　　　　　(d)

Figure 4. 2D slices showing the segmentation results of Figure 5. In (a) and (b) we show slices 50 and 90 used with the polyhedral model. In (c) and (d) we show the same slices from the segmentation result using a continuous active surface implemented with level set methods.

4.2 Applications

The active polyhedron excels at representing polyhedral shapes, but since triangle meshes are such a powerful shape representation, the method also is useful for representing more organic shapes, such as those found in medical imaging. The improved robustness to noise helps prevent erroneous segmentations.

In Figures 7 and 8 we demonstrate a segmentation of a darker structure in breast ultrasound data. Such structures are often candidates for tumor analysis in computer aided diagnosis applications. In (a) and (b) of each figure, we show the segmentation using a continuous active surface implemented with level set methods. As with the synthetic example in the previous subsection, the continuous surface breaks apart and takes on an irregular shape due to the speckle noise; so much so in Figure 8 that the result is nearly unusable. In (c) and (d) of each figure we show the result using the active polyhedron. As expected, the active polyhedron produces a much less ragged result due to its increased robustness. We have observed similar results with other noisy ultrasound images.

We used an active polyhedron to segment an atrial chamber from a 256^3 volume of cardiac ultrasound data. The results are shown in (a) and (b) of Figure 9. In (a), we show the 3D polyhedral surface overlaid with a slice through the volume, and in (b), we show the corresponding 2D slice.
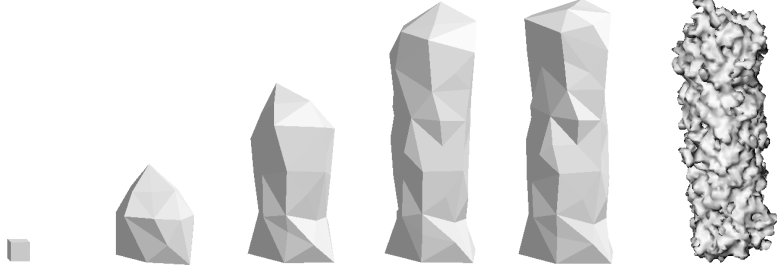
Figure 5. 3D segmentation using an active polyhedron. Left to right: 0**,** 10**,** 20**,** 30**, and** 35 **iterations (using a time step of** 1.0**). For comparison, on the far right is the segmentation result using a continuous active surface implemented with level set methods (using a time step of** 0.125 **to satisfy CFL conditions).**

Approach	Volume (units^3)	Surface Area (units^2)
Ground Truth	20106	4649
Continuous (Level sets)	21096	11510
Discrete (Active polyhedron)	19230	4867

Table 1. Volume and surface area, ground truth and estimated, for the ultrasound example of Figure 5.

(a)   (b)
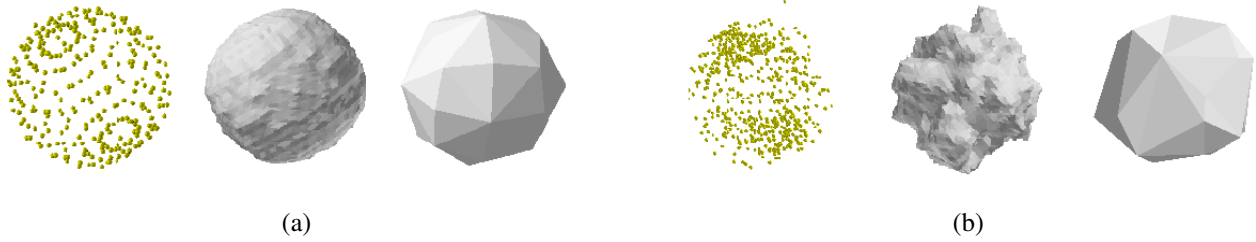
Figure 6. Reconstructing a polyhedral sphere from clean (a) and noisy (b) point cloud data. Left to right: Point cloud data, continuous reconstruction using level sets using a time step of 0.125**, discrete reconstruction using the active polyhedron using a time step of** 1.0**.**

As another example, we used an active polyhedron to segment the trachea from a 256 x 256 x 319 volume of lung CT data. The results are shown in (c) and (d) of Figure 9. In (c), we show the 3D polyhedral surface overlaid with a slice through the volume, and in (d), we show the corresponding 2D slice.

We reconstruct a surface of part of the human ear canal from point cloud data obtained by laser scanning a mold formed in a person's ear. The point cloud data was placed into a 128^3 volume and the active polyhedron was used reconstruct the surface at different resolutions, as shown in Figure 10. We run a similar experiment for reconstructing the Stanford bunny in Figure 11, that later of which shows

an example with more interesting geometry. As the resolution of the surface increases, more details emerge. As one further increases the resolution of the active polyhedron, finer surface details are modeled. However, for regularity and robustness to noise, the active polyhedron prefers well-separated vertices.

5 Conclusion

In this paper we presented a novel deformable surface, an active polyhedron, for 3D medical image segmentation, and additionally show its use in reconstructing surfaces from unorganized points. Starting with the general theory of surface
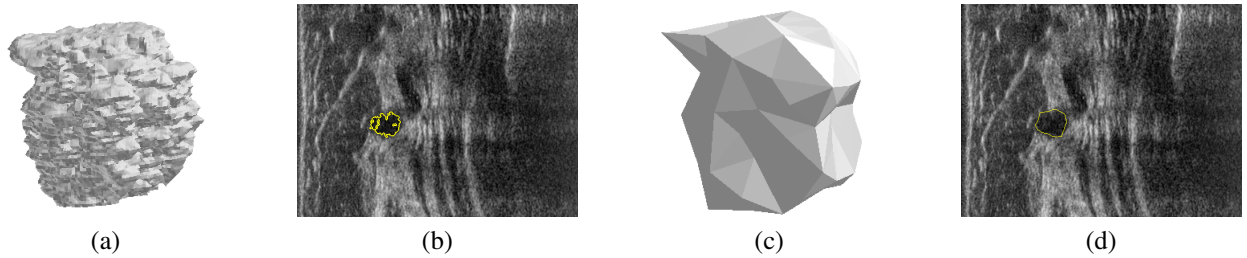
(a)   (b)   (c)   (d)

Figure 7. Using an active polyhedron to segment breast ultrasound data. We show a 3D segmentation using a continuous surface implemented with level set methods (a) and a slice through segmented volume (b). We repeat the experiment using the active polyhedron and show the results in (c) and (d).
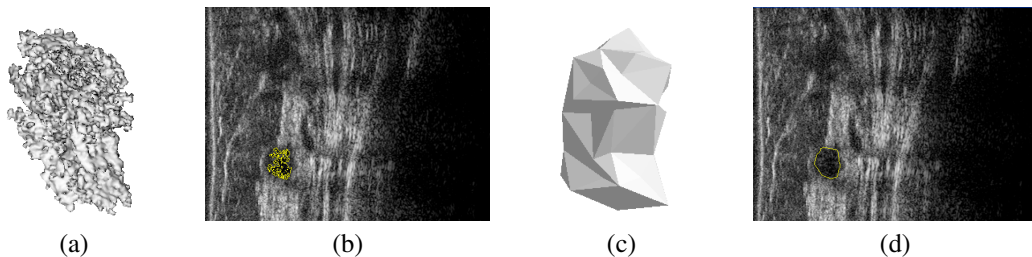

(a)   (b)   (c)   (d)

Figure 8. Another breast ultrasound example. Continuous surface (a) and (b), and active polyhedron (c) and (d). Note that the active polyhedron solution is much more robust.
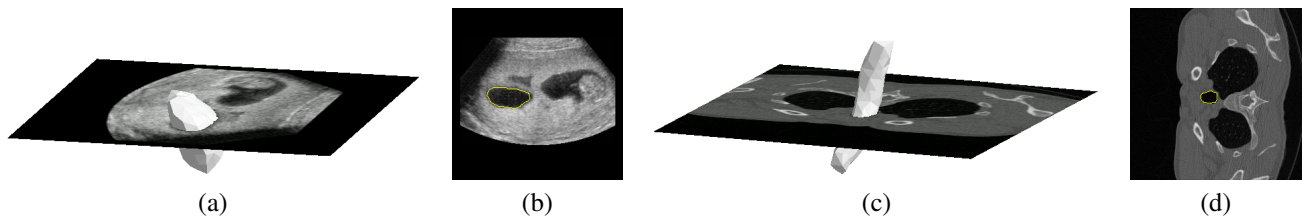

(a)   (b)   (c)   (d)

Figure 9. Using an active polyhedron to segment 3D medical data. In (a) and (b) we show a segmentation of an atrial chamber from ultrasound data, and in (c) and (d) we show a segmentation of the trachea from CT data. A time step of 1.0 was used in both evolutions.

evolution, we derived the equation of motion of a polyhedral surface by minimizing an energy functional using gradient descent. We also described an electrostatic regularizer that preserves sharper features but prevents the surface from self-intersecting. We then demonstrated the usefulness of an active polyhedron in segmenting noisy 3D medical images, as well as reconstruction from unorganized points, and offered a comparison to a continuous active surface implemented with level set methods. While more in-depth experimentation is required, from our results we conclude that the integration of the speed term over the active polyhe-

dron's faces results in significant robustness to noise. The increased time step one can use in the active polyhedron framework is an additional benefit that, depending on the number of triangles used in the mesh, can result in faster evolutions than narrowband level set methods. However, due to space constraints, we do not present runtime results in this paper.

Like many deformable surfaces, the active polyhedron described in this paper is capable of mesh refinement, but does not support topological changes. This is not necessarily a disadvantage, as in many applications the topology
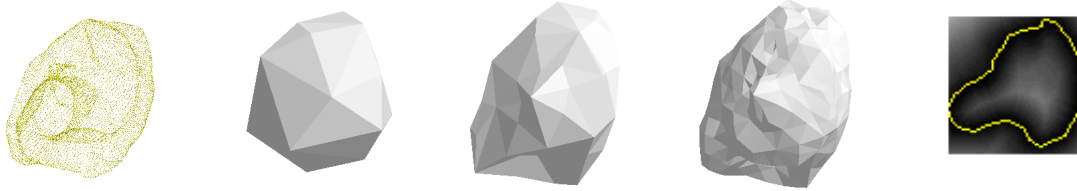
Figure 10. Using an active polyhedron to reconstruct a portion of a human ear canal shape. Left: point cloud. Next: reconstruction with edge length = 40**,** 25**, and** 10 **units. Right: slice going through distance volume upon convergence.**

Figure 11. Different resolutions of reconstructions of the Stanford Bunny from point cloud data. A time step of 1.0 **was used.**

of the object being segmented is known a priori, and topological changes are undesirable [5]. However, it would be possible to incorporate topological operations [4, 8, 11] into our model. This is left for future work.

The quality of the results of presented in this paper are dependent on the image-based terms we implement to evolve the active polyhedron, particularly for segmentation. More advanced functions that rely on higher order statistics, probabilistic measures, and textural properties [2, 13] will likely be required to further improve results. We believe that the active polyhedron framework is very promising and could also be applied to problems in object recognition, 3D tracking, and multi-view stereo reconstruction.

6   Acknowledgements

References

[1] B. Baillard and C. Barillot. Robust 3D Segmentation of Anatomical Structures with Level Sets. In *The Intl. Conf. on Medical Image Computing and Computer-Assisted Intervention*, pages 236–245, 2000.

[2] D. Boukerroui, O. Basset, A. Baskurt, and G. Gimenez. A multiparametric and multiresolution segmentation algorithm of 3-d ultrasonic data. *IEEE Trans. on Ultrasonics, Ferroelectrics, and Frequency Control*, 48(1):64–77, 2001.

[3] T. Chan and L. Vese. Active contours without edges. *IEEE Trans. on Image Processing*, 10(2):266–277, 2001.

[4] Y. Duan, L. Yang, H. Qin, and D. Samaras. Shape Reconstruction from 3D and 2D Data Using PDE-Based Deformable Surfaces. In *European Conference on Computer Vision*, volume III, pages 238–251, 2004.

[5] X. Han, C. Xu, and J. Prince. A topology preserving level set method for geometric deformable models. *IEEE Trans. on Patt. Anal. and Machine Intelligence*, 25(6):755–768, 2003.

[6] M. Kass, A. Witkin, and D. Terzopoulos. Snakes: Active contour models. *Intl. Journal of Computer Vision*, 1(4):321–331, 1987.

[7] J. Kraus. *Electromagnetics*. McGraw-Hill, New York, fourth edition, 1992.

[8] J. Lachaud and J.Montanvert. Deformable meshes with automated topology changes for coarse-to-fine 3d surface extraction. *Medical Image Analysis*, 3(2):187–207, 1999.

[9] R. Malladi, J. Sethian, and B. Vemuri. Shape modeling with front propagation: A level set approach. *IEEE Trans. on Patt. Anal. and Machine Intelligence*, 17(2):158–175, 1995.

[10] T. McInerney and D. Terzopoulos. Deformable models in medical image analysis: A survey. *Medical Image Analysis*, 1(2):91–108, 1996.

[11] T. McInerney and D. Terzopoulos. Topology adaptive deformable surfaces for medical image volume segmentation. *IEEE Trans. on Medical Imaging*, 18(10):840–850, 1999.

[12] G. Unal, H. Krim, and A. Yezzi. A Vertex-Based Representation of Objects in Images. In *IEEE Intl. Conference on Image Processing*, volume I, pages 896–899, 2002.

[13] G. Unal, A. Yezzi, and H. Krim. Information-theoretic active polygons for unsupervised texture segmentation. *The Intl. Journal of Computer Vision*, 62(3):199–220, 2005.

[14] R. Zaritsky, N. Peterfreund, and N. Shimkin. Velocity-guided tracking of deformable contours in three dimensional space. *The Intl. J. of Computer Vision*, 51(3):219–238, 2003.

[15] H. K. Zhao, S. Osher, and R. Fedkiw. Fast Surface Reconstruction Using the Level Set Method. In *Proc. IEEE Workshop on Variational and Level Set Methods (VLSM'01)*, pages 194–202, 2001.

[16] S. Zhu and A. Yuille. Region competition: Unifying snakes, region growing, and bayes/mdl for multi-band image segmentation. *IEEE Trans. on Patt. Anal. and Machine Intelligence*, 18(9):884–900, 1996.